Air-stable and High-Mobility n-Channel Organic Transistors based on Small-Molecule/Polymer Semiconducting Blends

By *Hongliang Zhong, Jeremy Smith, Stephan Rossbauer, Andrew J. P. White, Thomas D. Anthopoulos* and Martin Heeney**

[*] Dr H. Zhong, Dr M. Heeney
Centre for Plastic Electronics and Department of Chemistry
Imperial College London, SW7 2AZ (UK)
E-mail: m.heeney@imperial.ac.uk

[*] Dr J. Smith, Mr S. Rossbauer, Dr T. D. Anthopoulos
Centre for Plastic Electronics and Department of Physics
Blackett Laboratory, Imperial College London, SW7 2AZ (UK)
E-mail: thomas.anthopoulos@imperial.ac.uk

Dr A. J. P. White
Chemical Crystallography Laboratory
Department of Chemistry
Imperial College London, SW7 2AZ (UK)

Keywords: organic field-effect transistors, n-channel organic semiconductors, organic blend semiconductors

Although the performance of organic thin-film transistors (OTFTs) has increased significantly over the last decade, it still remains challenging to fabricate large area arrays of transistors with good device-to-device parameter uniformity.[1] Approaches based on the use of solution processable organic semiconductors are attractive, both in terms of throughput and the ability to pattern the semiconductor directly onto a range of substrate materials such as plastic. In terms of organic semiconductors, both soluble small molecules and polymers are viable materials classes with the former often being advantageous in terms of the higher charge carrier mobilities that can be obtained in OTFTs. Despite this significant advantage, however, the processing of highly crystalline small molecules into uniform thin films over large area substrates is often much more challenging than polymers, especially with respect to

device to device parameter spread. This is often related to the intrinsic anisotropy of transport in polycrystalline small molecules based films, in addition to pronounced grain boundary effects.[2] An attractive approach to these processing challenges is to combine the high mobility properties of small molecules with the advantageous processability of polymers and fabricate blend based OTFTs.[3] It has recently been shown that simple physical blending of a small molecule and a polymer matrix material affords control of the rate and degree of crystallization of the small molecule component during film formation. This has been successfully demonstrated with blends of several p-type organics, such as 6,13-bis(triisopropylsilylethynyl) pentacene (TIPS-pentacene)[4] and 2,8-difluoro-5,11-bis(triethylsilylethynyl)anthradithiophene (diF-TESADT),[5] in combination with different types of binder polymers. OTFTs fabricated from such semiconducting blends have shown hole mobilities over 5 $cm^2 V^{-1} s^{-1}$ with excellent device reproducibility.[5-6]

Despite the great potential of the small molecule-polymer blend approach, the methodology has yet to be applied to electron transporting (n-type) organic semiconducting systems. The demonstration of such materials and devices are a key element for the development of next generation large-scale integrated circuits based on complementary logic. Unfortunately, progress in the area of n-type organics has generally lagged the development of p-types, and there are far fewer examples of solution processable, high mobility n-type polymers and small molecules.[7] Of particular importance is the development of air stable materials i.e. compounds that are not susceptible to atmospheric oxidants such as oxygen and water. Several studies have suggested lowest unoccupied molecular orbital (LUMO) levels below -4 eV is necessary for air stable electron transport,[8] and the development of materials combining high mobility, good stability and solution processability has proved a particular challenge.

A promising class of small molecules that could potentially address the issues of deep LUMO level (i.e. ambient stability) and high electron mobility (high performance), are small molecule compounds based on diketopyrrolopyrrole (DPP) as the core building block.[9] The fused ring of DPP is known to have a strong tendency to stack in the solid state, possibly driven by very strong electrostatic and hydrogen bonding interactions. This rather unique property has recently been exploited for the demonstration of a number of high performing p-type as well as ambipolar DPP containing polymers.[10] On the contrary, small molecules based on simple DPP derivatives have so far been either p-type,[11] or displayed very low electron mobilities.[12] Inspired by the pioneering work of Otsubo and Takimiya on thienoquinoidal systems,[13] we speculated that the incorporation of dicyanomethylene groups onto the peripherary of a DPP containing small molecule would result in sufficient electron accepting character to stabilize the formation of an oxidised quinodal state (lowering of the LUMO), and therefore enhance the electron transport character of the molecule as well as its stability towards the various atmospheric oxidants.

We hereby report on a new soluble and highly air stable n-type organic semiconductor containing an oxidised DPP core. By combining this novel and solution processable small molecule with a carefully chosen insulating polymer, as the binder material, we are able to demonstrate, for the first time, blend OTFTs that exhibit both, high electron mobility (~0.5 cm^2/Vs) and excellent operating stability when exposed to ambient air for a prolonged period of time. To the best of our knowledge this is the first report of an air stable n-channel OTFT based on a semiconducting blend. The work could have significant implications for the development of solution-processed organic microelectronics based on complementary logic architectures.

Figure 1(a) displays the synthetic route adopted for the synthesis of the DPP derivative. Starting from 3,6-bis(5-bromo-2-thienyl)-2,5-dihexadecyl-2,5-dihydropyrrolo[3,4-

c]pyrrole-1,4-dione (DPP-Br), which was prepared according to literature procedure,[14] 2,2'-[(2,5-dihexadecyl-3,6-dioxo-2,3,5,6-tetrahydropyrrolo[3,4-*c*]pyrrole-1,4-diylidene)dithiene-5,2-diylidene]dimalononitrile (DPP-CN) was synthesized by a modified Takahashi reaction[15] . Typical Takahashi reaction conditions with 10% palladium catalyst were initially employed, however only low yields (10-20%) of the target molecule were obtained, accompanied by significant amounts of decomposition products that appeared to result from opening of the diketopyrrolopyrrole ring. The yield was significantly improved by performing the oxidative addition step with stoichiometric catalyst, prior to the subsequent addition of the anion of malononitrile. Under these conditions, significantly fewer degradation products were observed. The chemical structure of DPP-CN was confirmed by a combination of NMR, mass spectra and single crystal X-ray diffraction (*Supporting Information*).

The optical properties of DPP-CN were investigated by UV-vis absorption spectroscopy. **Figure 1(b)** displays the absorption spectra for the DPP-CN and DPP-Br in THF solutions and the DPP-CN film. The solution spectra of DPP-CN exhibits a vibronic structure common to many DPP dyes,[16] with a maximum at 638 nm and a shoulder at 615 nm. This represents a ca. 80 nm red shift in comparison to the starting DPP-Br material (shoulder at 525 nm, maximum at 566 nm). In the solid state the spectrum broadens and red shifts, with a maxima at 663 nm and a shoulder at 734 nm, suggestive of enhanced π-π interactions. The optical band gap of DPP-CN film was estimated from the onset of absorption yielding a value of ~1.5 eV.

The redox behavior of DPP-CN was characterized by electrochemical cyclic voltammetry (CV) [**Figure 1(c)**]. DPP-CN shows excellent reversible reduction behavior with two reduction peaks, but no obvious oxidation peak was observed. The LUMO value of DPP-CN is estimated at -4.2 eV by the onset of the reduction peak, which is sufficiently low

to expect air stable electron transport to occur.[8b, 17] The HOMO level has also been estimated at -5.7 eV by subtracting the optical band gap from the reduction potential.

The molecular packing of DPP-CN was investigated in single crystals by x-ray diffraction [**Figure 1(d-e)**].The X-ray diffraction data demonstrates that there is a slight twist in the molecule, with an angle of *ca*. 7° about the bond between the thiophene ring and the DPP core. Both the thiophene ring and the DPP distort to accommodate the quinodal structure, with for example the central C–C bond of the DPP ring shortening to 1.355(4) Å from a distance of 1.422 Å[18] as it takes double bond character. **Figure 1(d)** shows how adjacent molecules are linked by π···π and C=O···C≡N interactions to form a sheet in the *ab* plane. The $C_{16}H_{33}$ alkyl chains of adjacent sheets interdigitate, as shown in **Figure 1(e)** to form lamella like structures. The π···π interaction between a diketopyrrolopyrrole ring in one molecule and a thiophene in the next [interaction **a** in **Figure 1(d)**] has centroid···centroid and mean interplanar separations of *ca*. 3.89 and 3.30 Å respectively, the two five-membered rings being inclined by *ca*. 10°, and forms a stack of molecules along the *a* axis direction (*see also Supporting Information*). The C=O···C≡N contact [interaction **b** in **Figure 1(d)**] has a centroid···centroid separation of *ca*. 3.09 Å, and forms an extended chain along the crystallographic [1,-1,0] direction (*see also Supporting Information*). The close molecular contacts and extended two dimensional order in the crystal suggest DPP-CN is a promising material for OFET applications.

The surface morphology and electrical properties of blend films of DPP-CN:poly(α-methyl styrene) (PαMS) have been studied using high resolution atomic force microscopy (AFM) and thin-film transistor measurements. It is worth mentioning that attempts to spin cast the neat DPP-CN solution onto Si^{++}/SiO_2 substrates, treated with hexamethyldisilazane (HMDS), failed to produce any continuous film due to the very low surface energy of the solution and the substrate surface. Spin casting of the DPP-CN: PαMS blend on the other

hand was found to produce good quality films with high and long-range uniformity. **Figures 2(a)** show the polarized light microscopy images of the DPP-CN:PαMS films. From this image it appears that the blend films, under un-optimized deposition conditions, exhibit two phases, one consisting of larger [region A, **Figure 2(a)**] and one of smaller [region B, **Figure 2(a)**] spherulitic-like grains. **Figure 2(b)** displays the magnified image of region A shown in **Figure 2(a)**.

Figure 2(c-d) shows representative AFM images for the two film regions (large and small grains) while **Figure 2(e)** displays the statistical distributions of their surface height evaluated from the topography AFM measurements. Both film regions exhibit large surface roughness of 26.2 nm to 47.3 nm for the large and small grain region, respectively. We attribute this to the segregation and crystallization of DPP-CN molecules at the surface (film/air interface) of the blend film. Such distinct phase separation has been seen previously in hole transporting blends containing the small molecule diF-TESADT, as well as TIPS-pentacene, and polystyrene as the polymer binder.[4] Interestingly, the large grain regions exhibit a lower roughness as well as a narrower distribution of heights [**Figure 2(e)**] most likely due to the improved regularity and size of the spherulitic crystalline domains.

The electronic properties of the DPP-CN:PαMS film's surface (shown in **Figure 2**) have been studied using carefully engineered top-gate, bottom-contact (TG-BC) transistor architectures. **Figure 3(a)** displays the TG-BC transistor structure used. The specific architecture provides a unique tool for studying the electronic properties of the film's top surface in a non-destructive manner since solution processing of CYTOP is performed using an orthogonal fluorinated solvent. The experimental procedures related to device preparation are reported in the *Experimental* section. Despite the highly rough surface of the DPP-CN:PαMS films [**Figure 2(c-e)**], the TG-BC transistors exhibit promising electronic characteristics as evident from the transfer and output characteristics shown in **Figures 3(b)**

and **3(c)**, respectively. The channel current on/off ratio measured from these devices is relatively low with maximum values in the range 10^3-10^4. The latter is most likely attributed to the very rough blend semiconductor/CYTOP interface [see **Figure 2(c-d)]**. It has recently been shown that in the case of p-channel blend OTFTs, smoother semiconductor/dielectric interface leads to higher hole mobilities and higher channel current on/off ratio.[5] It is therefore anticipated that improvements in the interface quality through processing improvements could lead to both improved electron transport and current on/off ratio. The maximum electron mobility (μ_e) measured in the linear and saturation operating regimes was similar and on the order of ~0.5 cm^2/Vs. To the best of our knowledge this is one of the highest electron mobility values reported to date for solution-processed OTFTs,[19] and the first example of a n-channel blend-based OTFT. The observation of high transistor performance in the presence of an extremely rough interface is counterintuitive since previous studies performed on pentacene OTFTs have reported a negative dependence of hole mobility with increasing interface roughness.[20] It is worth noting, however, that the latter studies were performed on bottom-gate, top-contact (BG-TC) transistor architectures where the surface energy of the dielectric can dramatically affect the growth of the organic layer and hence the electronic characteristics of the first few monolayers. An interesting conclusion that can be drawn from this observation is that top-gate OTFTs based on blend semiconductors appear remarkably immune to the semiconductor/insulator interface morphology and more specifically its roughness. Elucidating the exact mechanism however responsible for this observation would require further work and is beyond the scope of this work.

The linear dependence of the channel current (I_D) on drain voltages (V_D), at low bias, in **Figure 3(c)** indicates a rather good electron injection to the LUMO level of DPP-CN despite the significant mismatch between the Fermi energy level of the Au (-4.8 eV) source-drain (S-D) electrodes and the LUMO of DPP-CN (-4.2 eV). This is most likely due to either

slightly higher work function of the Au electrodes and/or to a deeper, i.e. more negative, LUMO level in the solid-state DPP-CN film (cyclic voltammetry was performed in solution, **Figure 1(c)**]. Such shift in the energetics of the organic semiconductor is not surprising and can be attributed to strong intermolecular interactions between DPP-CN units [see **Figure 1(b-d)**].

The rather deep LUMO energy level of DPP-CN prompted us to investigate the stability of electron transport towards ambient air. We have previously shown that lowering of the LUMO energy level below -4 eV results to air-stable electron transport.[8a] For the purpose of this experiment, as-prepared DPP-CN:PαMS based transistors [**Figure 3(a**)] were exposed to ambient air for one day while their electrical characteristics were measured at regular intervals. **Figure 4(a)** displays the evolution of the electron mobility with exposure time for a number of DPP-CN:PαMS based transistors. The transfer characteristics obtained from one of the OTFTs after being exposed to ambient air for 1300 minutes is shown in **Figure 4(b)**. It can be seen from these data that the transistor characteristics do not change significantly, with the electron mobility and current on/off ratio remaining very constant throughout the exposure period. To the best of our knowledge the present results are among the best sets of data reported to date for solution processed n-channel OTFTs both in terms of carrier mobility and ambient stability.

In summary, we have reported the synthesis of a novel electron transporting small-molecule organic semiconductor containing a reduced DPP core. Thin films based on blends of the DPP-CN derivative and the insulating polymer PαMS, used as a binder, were found to exhibit strong vertical phase separation with the DPP molecule diffusing and crystallizing on the surface of the composite film. Using carefully engineered top-gate transistor architectures we have been able to evaluate the electronic properties of the DPP-CN rich film surface. As-prepared transistors yield maximum electron mobilities on the order of 0.5 cm^2/Vs and

current on/off ratio in the range 10^2-10^3. Importantly, the n-channel DPP-CN based OTFTs exhibit air-stable operation, a characteristic attributed to the very low lying LUMO level of the novel DPP-CN molecule.

Experimental

General: Commercially available reagents were purchased and used without further purification unless otherwise stated. All solvents were dehydrated and syringes which were used to transfer reagents or solvents were purged with Argon prior to use. ^{1}H NMR spectra were recorded on Bruker AV-400 spectrometer using $CDCl_3$ as solvent and TMS as internal standard. ^{13}C NMR spectra were obtained on Bruker DRX400 with $CDCl_3$ at 50 ^{o}C. Mass spectra were taken with Micromass MALDI micro MX. Elemental analysis was performed with a Thermo EA1108 or FlashEA1112 elemental analyzer. UV-vis spectra were recorded with a PerkinElmer Lambda20 UV-vis spectrophotometer. IR was determined by PerkinElmer Spectrum 100 FT-IR Spectrometer. Flash chromatography (FC) was carried out on silica gel (Merck Kieselgel 60 grade 40−63 μm F254) using flash techniques. Analytical thin layer chromatography (TLC) was performed on Merck Kieselgel 60 F254 aluminum sheets and visualization was effected with UV fluorescence (254 and 365 nm). Cyclic voltammetry was determined in a DCM solution containing tetrabutylammonium hexafluorophosphate (0.10 M) with a scanning rate of 0.1V s^{-1} at room temperature. A standard three-electrode using a platinum wire working electrode, a platinum mesh counter electrode and a silver wire reference electrode was employed. The reduction potentials were calibrated with a ferrocene/ferrocenium (FOC) redox system as the standard (assuming the HOMO energy level of FOC is 4.8 eV below vacuum).

Synthesis: A solution of malononitrile (0.30 g, 4.5 mmol) in anhydrous THF (10 mL) was added dropwise to a suspension of sodium hydride (0.16 g, 60%, 4.0 mmol) in 10 mL THF at 0 ^{o}C under argon atmosphere. The reactant was allowed to warm to room temperature and reserved to use. DPP-Br (0.36 g, 0.4 mmol) and tetrakis(triphenylphosphine)palladium (0.92 g, 0.8 mmol) were dissolved in 15 mL THF, and then stirred for 30 minutes at reflux, followed by the dropwise addition of the prepared malononitrile anion solution. After reflux overnight, the reaction mixture was cooling to 0°C and exposed to air. Dilute hydrochloric acid (20 mL) was added, followed by stirring for 30 minutes at 0°C. The mixture was subsequently extracted with diethyl ether (50 mL) and organic phase was separated, washed with water, dried over anhydrous Mg_2SO_4 and concentrated. The crude product was purified by flash chromatography on silica gel (eluent: DCM) to afford DPP-CN (0.22 g, 0.25 mmol, 63%) as a dark green solid.

^{1}H NMR (400 MHz, $CDCl_3$, δ): 9.38 (d, J = 5.6 Hz, 2H), 7.39 (d, J = 6.0 Hz, 2H), 4.07 (t, J_1 = 15.6 Hz, J_2 = 7.8 Hz, 4H), 1.73 (m, 4H), 1.42-1.36 (m, 8H), 1.25 (br, 44H), 0.87 (t, J_1 = 13.6 Hz, J_2 = 6.8 Hz, 6H). ^{13}C NMR (100 MHz, $CDCl_3$, δ): 172.4, 161.1, 146.8, 135.3, 133.3, 131.4, 130.6, 113.1, 112.2, 71.6, 43.0, 31.9, 30.0, 29.7, 29.6, 29.5, 29.4, 29.3, 29.1, 26.7, 22.7, 14.0. MS (MALDI, *m/z*): $[M + H]^+$ 876. Anal. Calcd for $C_{52}H_{70}N_6O_2S_2$: C, 71.35; H, 8.06; N, 9.60; S, 7.33. Found: C, 70.86; H, 8.04; N, 9.52; S, 7.35. FT-IR (ATR, cm^{-1}): 2918, 2850, 2214, 1688, 1498, 818.

Transistor fabrication and characterisation: Top-gate, bottom-contact devices were fabricated on glass with evaporated 30 nm thick gold source and drain contacts. The semiconductor blend was a 1:1 by weight DPP-CN:poly(α-methyl styrene) (PαMS) solution in tetrahydronaphthalene at 20 mg/ml total solid concentration. PαMS had a number average molecular weight (Mn) of 100 kDa and a PDI of 1.02 (Aldrich). The blend solution was heated and stirred at 160 °C to ensure it was fully dissolved before spin coating onto a hot substrate from hot solution in the temperature range 125-160 °C. Spin coating was carried out

at 500 rpm for 10 s followed by 2000 rpm for 20 s. The samples were then briefly dried at the same temperature to remove residual solvent. The fluoropolymer dielectric, CYTOP, (900 nm) was spin cast onto the semiconductor and annealed at 100 °C before aluminum gate electrodes were deposited by thermal evaporation. OTFTs were fabricated and tested in nitrogen. Electrical measurements were carried out using a Keithley 4200 semiconductor parameter analyser. Air stability was tested by exposing the devices to ambient air (~60% humidity) and measuring transfer characteristics over a period of 1 days. Basic electrical measurements were performed in a nitrogen atmosphere. The electron mobility was estimated using the standard thin film transistor model in both linear and saturation regimes of the device.

Microscopy: Atomic force microscopy (AFM) was carried out using an Agilent 5500 in close-contact (tapping) mode and both topography and phase images were recorded. Polarized optical microscopy (POM) images were taken in transmission using a Nikon LV100 both of simple films on glass as well as complete OTFT structures.

Acknowledgements

This work was funded by the Engineering and Physical Sciences Research Council (EPSRC) grant numbers EP/F023200, EP/F065884/1, EP/I002936/1 and EP/G060738/1 and Research Councils UK (RCUK). T.D.A. is an EPSRC Advanced Fellow and a RCUK fellow.

Received: ((will be filled in by the editorial staff))
Revised: ((will be filled in by the editorial staff))
Published online: ((will be filled in by the editorial staff))

References

[1] a) Y. Wen, Y. Liu, Y. Guo, G. Yu, W. Hu, *Chem. Rev.* **2011**, *111*, 3358; b) A. C. Arias, J. D. MacKenzie, I. McCulloch, J. Rivnay, A. Salleo, *Chem. Rev*. **2010**, *110*, 3. c) P. M. Beaujuge, J. M. J. Frechet, *J. Am. Chem. Soc.* **2011**, *133*, 20009; d) Y. Wen, Y. Liu, *Adv. Mater.* **2010**, *22*, 1331; e) H. Sirringhaus, *Adv. Mater.* **2009**, *21*, 3859.

[2] a) A. A. Virkar, S. Mannsfeld, Z. A. Bao, N. Stingelin, *Adv. Mater.* **2010**, *22*, 3857; b) J. Rivnay, L. H. Jimison, J. E. Northrup, M. F. Toney, R. Noriega, S. F. Lu, T. J. Marks, A. Facchetti, A. Salleo, *Nat. Mater.* **2009**, *8*, 952-958.

[3] J. Smith, R. Hamilton, I. McCulloch, N. Stingelin-Stutzmann, M. Heeney, D. D. C. Bradley, T. D. Anthopoulos, *J. Mater. Chem.* **2010**, *20*, 2562-2574.

[4] a) J. Smith, R. Hamilton, M. Heeney, D. M. de Leeuw, E. Cantatore, J. E. Anthony, I. McCulloch, D. D. C. Bradley, T. D. Anthopoulos, *Appl. Phys. Lett.* **2008**, *93, 253301*; b) T. Ohe, M. Kuribayashi, R. Yasuda, A. Tsuboi, K. Nomoto, K. Satori, M. Itabashi, J. Kasahara, *Appl. Phys. Lett.* **2008**, *93, 053303*; c) M. B. Madec, D. Crouch, G. R. Llorente, T. J. Whittle, M. Geoghegan, S. G. Yeates, *J. Mater. Chem.* **2008**, *18*, 3230 d) J. Kang, N. Shin, D. Y. Jang, V. M. Prabhu, D. Y. Yoon, *J. Am. Chem. Soc.* **2008**, *130*, 12273.

[5] a) R. Hamilton, J. Smith, S. Ogier, M. Heeney, J. E. Anthony, I. McCulloch, J. Veres, D. D. C. Bradley, T. D. Anthopoulos, *Adv. Mater.* **2009**, *21*, 1166. b) J. Smith , W. Zhang , R. Sougrat , K. Zhao , R. Li , D. Cha, A. Amassian , M. Heeney , I. McCulloch , T. D. Anthopoulos, *Adv. Mater.* **2012,** DOI: 10.1002/adma.201200088.

[6] M. B. Madec, P. J. Smith, A. Malandraki, N. Wang, J. G. Korvink, S. G. Yeates, *J. Mater. Chem.* **2010**, *20*, 9155.

[7] a) H. Usta, A. Facchetti, T. J. Marks, *Acc. Chem. Res.* **2011**, *44*, 501; b) Y. G. Wen, Y. Q. Liu, *Adv. Mater.* **2010**, *22*, 1331; c) J. E. Anthony, A. Facchetti, M. Heeney, S. R. Marder, X. W. Zhan, *Adv. Mater.* **2010**, *22*, 3876.

[8] a) T. D. Anthopoulos, F. B. Kooistra, H. J. Wondergem, D. Kronholm, J. C. Hummelen, D. M. de Leeuw, *Adv. Mater.* **2006**, *18*, 1679; b) T. D. Anthopoulos, G. C. Anyfantis, G. C. Papavassiliou, D. M. de Leeuw, *Appl. Phys. Lett.* **2007**, *90*, 122105; c) D. M. de Leeuw, M. M. J. Simenon, A. R. Brown, R. E. F. Einerhand, *Synth. Met.* **1997**, *87*, 53; d) B. A. Jones, A. Facchetti, M. R. Wasielewski, T. J. Marks, *J. Am. Chem. Soc.* **2007**, *129*, 15259.

[9] Z. Hao, A. Iqbal, *Chem. Soc. Rev.* **1997**, *26*, 203.

[10] S. Qu, H. Tian, *Chem. Commun.* **2012,** *48*, 3039.

[11] S.-L. Suraru, U. Zschieschang, H. Klauk, F. Wurthner, *Chem. Commun.* **2011**, *47*, 1767.

[12] B. P. Karsten, J. C. Bijleveld, R. A. J. Janssen, *Macromol. Rap. Commun.* **2010**, *31*, 1554.

[13] a) T. Takahashi, K. I. Matsuoka, K. Takimiya, T. Otsubo, Y. Aso, *J. Am. Chem. Soc.* **2005**, *127*, 8928; b) T. M. Pappenfus, J. D. Raff, E. J. Hukkanen, J. R. Burney, J. Casado, S. M. Drew, L. L. Miller, K. R. Mann, *J. Org. Chem.* **2002**, *67*, 6015-6024; c) T. M. Pappenfus, R. J. Chesterfield, C. D. Frisbie, K. R. Mann, J. Casado, J. D. Raff, L. L. Miller, *J. Am. Chem. Soc.* **2002**, *124*, 4184; d) K. Yui, Y. Aso, T. Otsubo, F. Ogura, *Bull. Chem. Soc. Jpn.* **1989**, *62*, 1539; e) Y. Suzuki, M. Shimawaki, E. Miyazaki, I. Osaka, K. Takimiya, *Chem. Mat.* **2011**, *23*, 795 f) Y. Suzuki, E. Miyazaki, K. Takimiya, *J. Am. Chem. Soc.* **2010**, *132*, 10453.

[14] T. L. Nelson, T. M. Young, J. Liu, S. P. Mishra, J. A. Belot, C. L. Balliet, A. E. Javier, T. Kowalewski, R. D. McCullough, *Adv. Mater.* **2010**, *22*, 4617-4621.

[15] M. Uno, K. Seto, S. Takahashi, *J. Chem. Soc., Chem. Commun.* **1984**, 932.

[16] H. Bürckstümmer, A. Weissenstein, D. Bialas, F. Würthner, *J. Org. Chem.* **2011**, *76*, 2426.

[17] H. Usta, C. Risko, Z. Wang, H. Huang, M. K. Deliomeroglu, A. Zhukhovitskiy, A. Facchetti, T. J. Marks, *J. Am. Chem. Soc.* **2009**, *131*, 5586.
[18] J. Mizuguchi, A. Grubenmann, G. Wooden, G. Rihs, *Acta. Cryst.* **1992**, *B48*, 696.
[19] a) S. Fabiano, H. Wang, C. Piliego, C. Jaye, D. A. Fischer, Z. H. Chen, B. Pignataro, A. Facchetti, Y. L. Loo, M. A. Loi, *Adv. Funct. Mater.* **2011**, *21*, 4479; b) J. Li, J.-J. Chang, H. S. Tan, H. Jiang, X. Chen, Z. Chen, J. Zhang, J. Wu, *Chem. Sci.* **2012**, *3*, 846; c) X. Gao, C.-a. Di, Y. Hu, X. Yang, H. Fan, F. Zhang, Y. Liu, H. Li, D. Zhu, *J. Am. Chem. Soc.* **2010**, *132*, 3697; d) C. Piliego, D. Jarzab, G. Gigli, Z. Chen, A. Facchetti, M. A. Loi, *Adv. Mater.* **2009**, *21*, 1573.e) L. E. Polander, S. P. Tiwari, L. Pandey, B. M. Seifried, Q. Zhang, S. Barlow, C. Risko, J.-L. Brédas, B. Kippelen, S. R. Marder, *Chem. Mater.* **2011**, *23*, 3408.
[20] a) S. E. Fritz, T. W. Kelley, C. D. Frisbie, *J. Phys. Chem. B* **2005**, *109*, 10574; b) S. Steudel, S. De Vusser, S. De Jonge, D. Janssen, S. Verlaak, J. Genoe, P. Heremans, *Appl. Phys. Lett.* **2004**, *85*, 4400.

Figure Captions

Figure 1. (a) Synthetic route to DPP-CN. (b) UV-vis absorption spectra of DPP-CN and DPP-Br in THF solution and solid film. **(c)** Electrochemical cyclic voltammetry curve of DPP-CN in DCM solution containing tetrabutylammonium hexafluorophosphate (0.10 M) with a scanning rate of 0.1V s^{-1} at room temperature. (d) The crystal structure of **DPP-CN** showing part of one of the sheets of π···π and C=O···C≡N linked molecules in the *ab* plane (the terminal $C_{15}H_{31}$ units have been removed for clarity). The π···π interaction [**a**] has centroid···centroid and mean interplanar separations of *ca*. 3.89 and 3.30 Å respectively, the two five-membered rings being inclined by *ca*. 10°. The C=O···C≡N interaction [**b**] has a centroid···centroid separation of *ca*. 3.09 Å. (e) The crystal structure of **DPP-CN** showing the interdigitation of the $C_{16}H_{33}$ alkyl chains of adjacent sheets.

Figure 2. Polarized light microscopy (PLM) images of the DPP-CN:PαMS films. (a) Image of the blend film showing the existence of crystalline regions consisting of large (region A) and small (region B) spherulitic crystals. (b) Magnified image (20 × 20 μm) of region A shown in (a). AFM images for the film surface of the large crystal region A (c) and the small crystal region B (d) (scale bar = 4 μm). (e) Statistical distributions of surface height evaluated from the AFM topography images shown in c-d.

Figure 3. (a) The top-gate, bottom-contact (TG-BC) transistor architecture employed in this work. (b) Representative transfer characteristics obtained from a DPP-CN:PαMS top-gate transistor at V_D = 5 V and V_D = 60 V. (c) Output characteristics measured for the same transistor. Transistor channel length (L) and width (W) were 50 μm and 1 mm, respectively.

Figure 4. (a) Evolution of electron mobility, measured in saturation, as a function of exposure time to ambient air (RH ~ 60 %) for a DPP-CN:PαMS TG-BC transistor. (b) Transfer characteristics of the same blend transistor measured after exposure to ambient air for 1300 minutes. The transistor channel length (L) and width (W) were 50 μm and 1 mm, respectively.

Figure 1

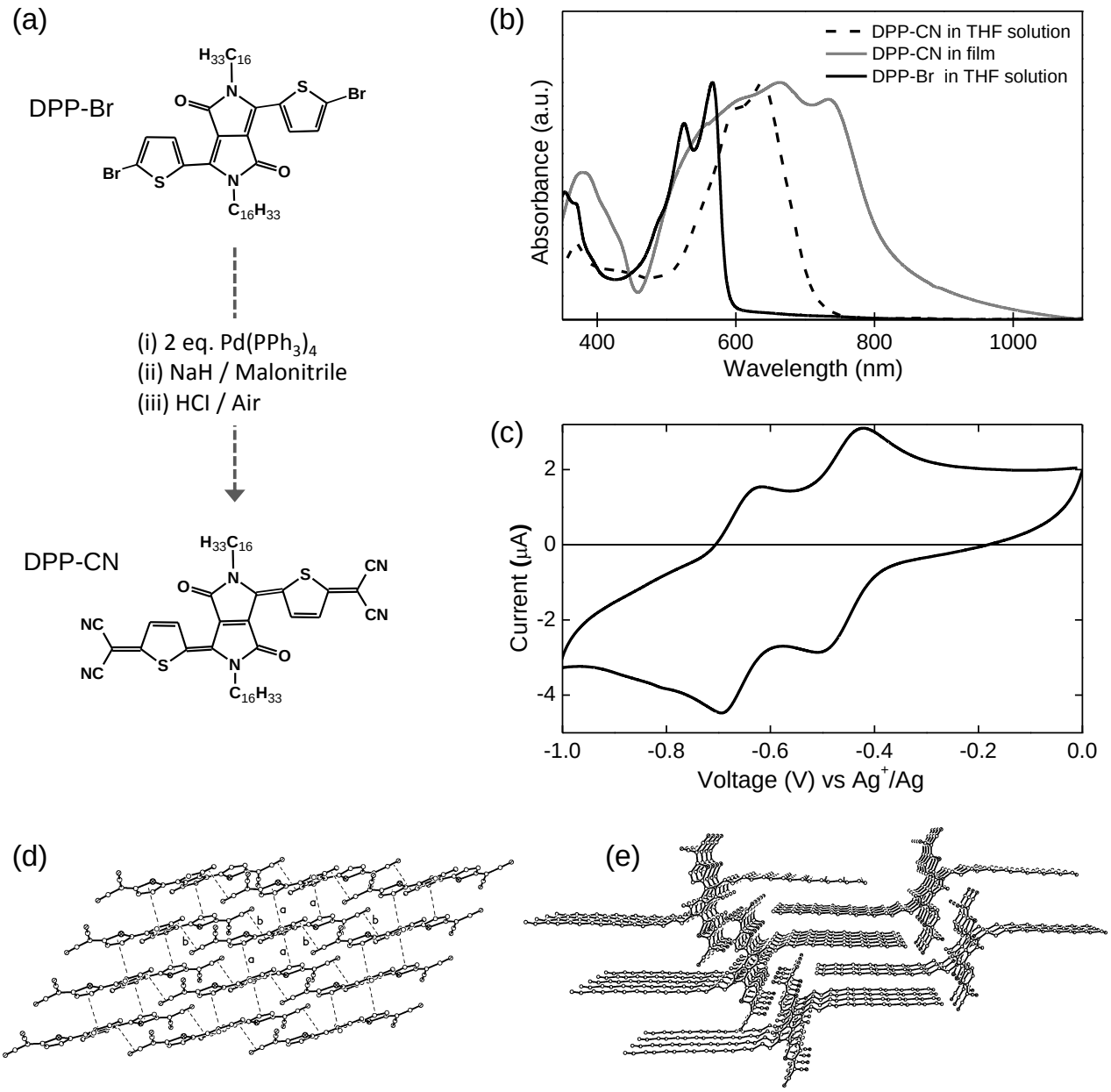
(a)
DPP-Br
(i) 2 eq. Pd(PPh3)4
(ii) NaH / Malonitrile
(iii) HCl / Air
DPP-CN
(b)
DPP-CN in THF solution
DPP-CN in film
DPP-Br in THF solution
Absorbance (a.u.)
Wavelength (nm)
(c)
Current (μA)
Voltage (V) vs Ag+/Ag
(d)
(e)

Figure 2

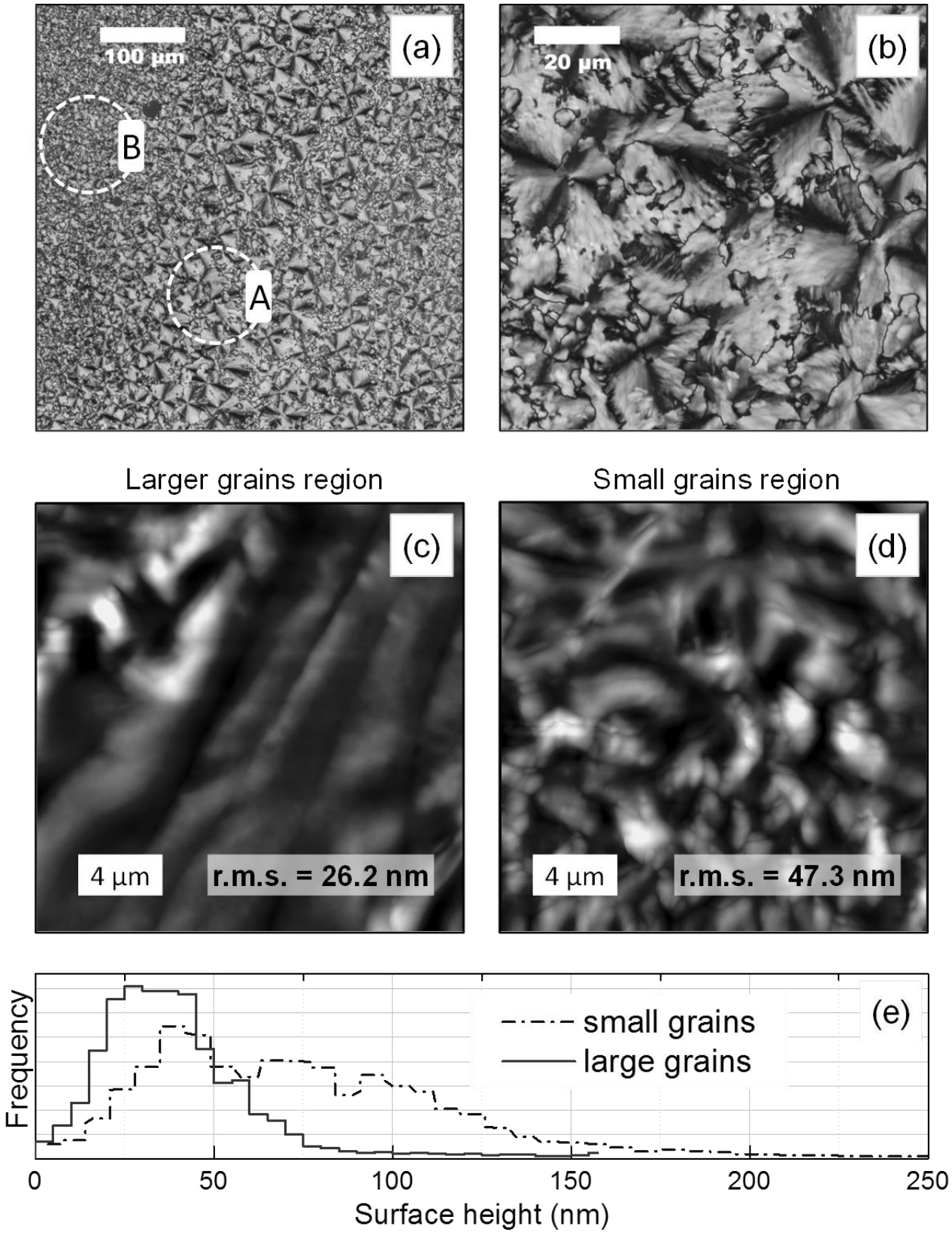
100 µm
(a)
B
A
20 µm
(b)
Larger grains region
Small grains region
(c)
4 µm
r.m.s. = 26.2 nm
(d)
4 µm
r.m.s. = 47.3 nm
Frequency
small grains
large grains
(e)
0
50
100
150
200
250
Surface height (nm)

Figure 3

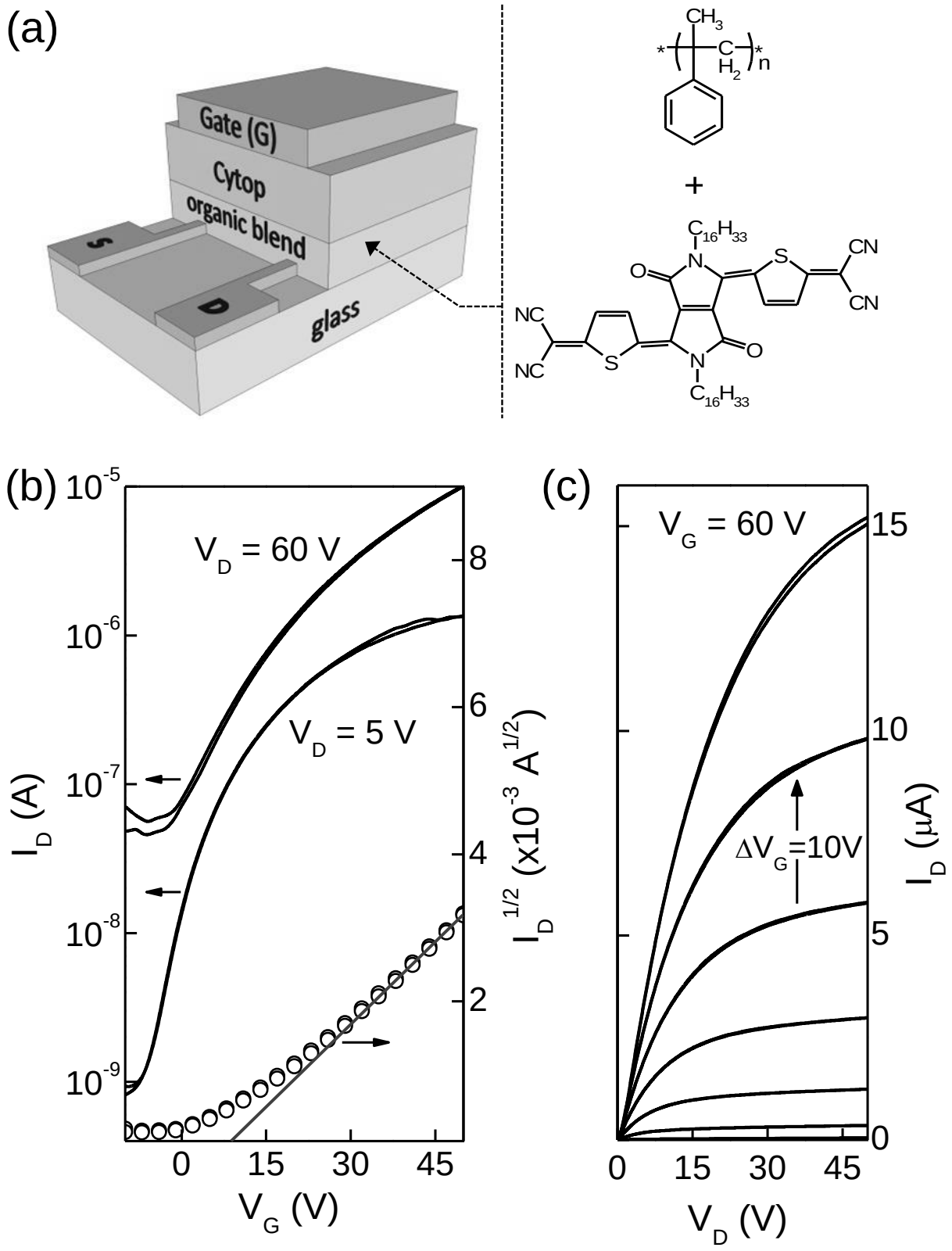
(a)
Gate (G)
Cytop
organic blend
S
D
glass
CH3
C
H2
n
+
C16H33
N
O
S
CN
CN
NC
NC
S
N
O
C16H33
(b)
10-5
10-6
10-7
10-8
10-9
VD = 60 V
VD = 5 V
ID (A)
8
6
4
2
ID1/2 (x10-3 A1/2)
0
15
30
45
VG (V)
(c)
VG = 60 V
ΔVG=10V
15
10
5
0
ID (μA)
0
15
30
45
VD (V)

Figure 4

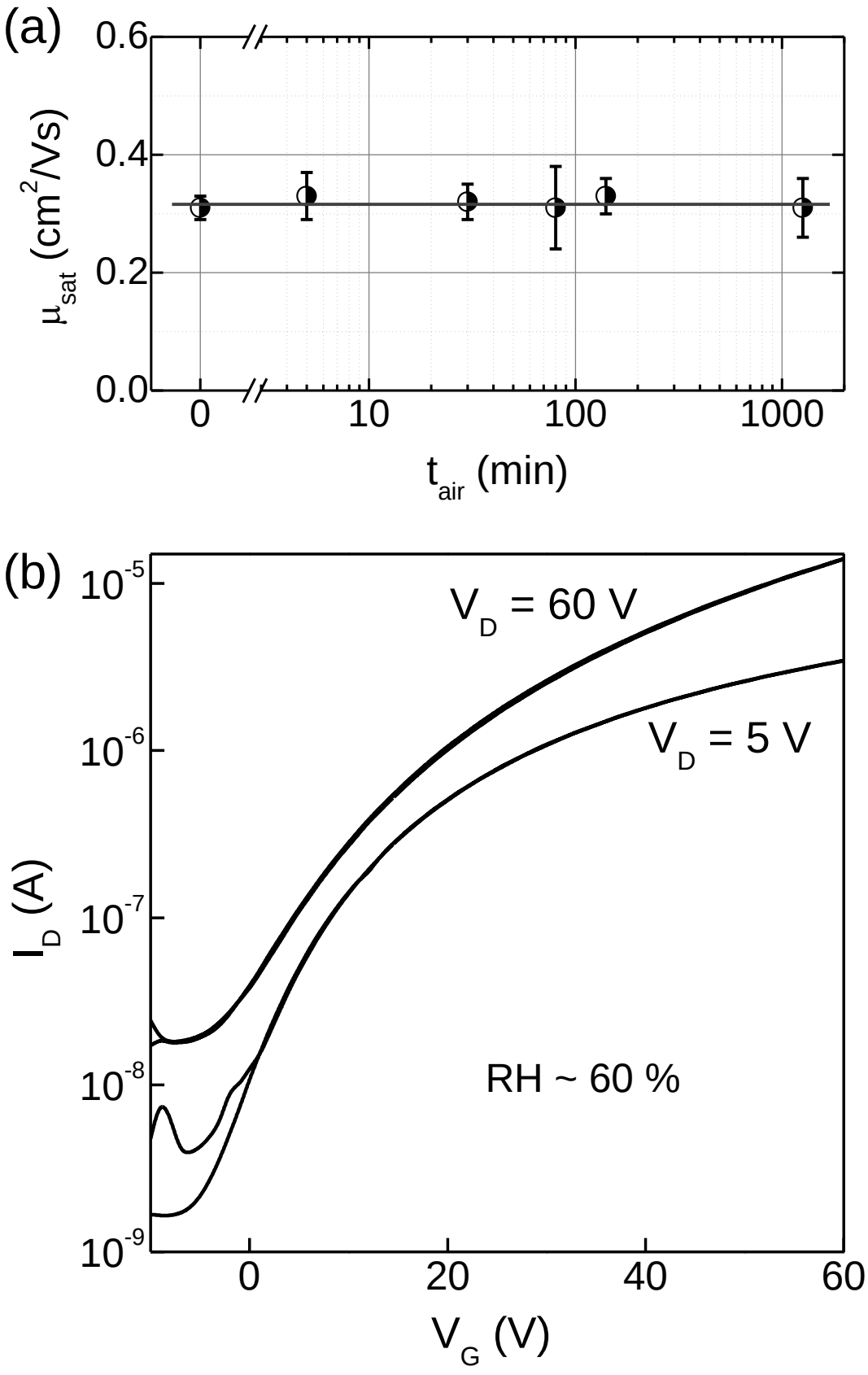
(a)
0.6
0.4
0.2
0.0
μsat (cm2/Vs)
0
10
100
1000
tair (min)
(b)
10-5
10-6
10-7
10-8
10-9
ID (A)
VD = 60 V
VD = 5 V
RH ~ 60 %
0
20
40
60
VG (V)